

Fragility of the fractional quantum spin Hall effect in quantum gases

O. Fialko¹, J. Brand¹, U. Zülicke²

¹ Institute of Natural and Mathematical Sciences and Centre for Theoretical Chemistry and Physics, Massey University, Auckland 0632, New Zealand

² School of Chemical and Physical Sciences and MacDiarmid Institute for Advanced Materials and Nanotechnology, Victoria University of Wellington, PO Box 600, Wellington 6140, New Zealand

E-mail: uli.zuelicke@vuw.ac.nz

Abstract. We consider the effect of contact interaction in a prototypical quantum spin Hall system of pseudo-spin-1/2 particles. A strong effective magnetic field with opposite directions for the two spin states restricts two-dimensional particle motion to the lowest Landau level. While interaction between same-spin particles leads to incompressible correlated states at fractional filling factors as known from the fractional quantum Hall effect, these states are destabilized by interactions between opposite spin particles. Exact results for two particles with opposite spin reveal a quasi-continuous spectrum of extended states with a large density of states at low energy. This has implications for the prospects of realizing the fractional quantum spin Hall effect in electronic or ultra-cold atom systems. Numerical diagonalization is used to extend the two-particle results to many bosonic particles and trapped systems. The interplay between an external trapping potential and spin-dependent interactions is shown to open up new possibilities for engineering exotic correlated many-particle states with ultra-cold atoms.

PACS numbers: 73.43.-f, 67.85.Fg, 71.70.Ej, 72.25.-b

Submitted to: *New J. Phys.*

1. Introduction

Trapped ultra-cold atoms have become model systems of choice for simulating physical effects from condensed matter [1] to cosmology [2, 3]. The recently achieved ability to create synthetic vector potentials [4] acting on neutral atoms has increased the versatility of the atomic-physics simulation toolkit even further. It is now possible to simulate magnetic fields by inducing spatially varying $U(1)$ (i.e., scalar) gauge potentials [5–7], and pseudo-spin splittings can be created in spinor gases [8, 9] using spatially constant vector potentials having a (possibly non-Abelian) matrix structure. These advances have stimulated a host of theoretical works studying, e.g., the effect of uniform $SU(2)$ gauge potentials on the behavior of quantum particles subject to uniform ordinary magnetic fields [10–13], or proposing the use of staggered effective spin-dependent magnetic fields in optical lattices [14–17] to simulate a new class of materials called topological insulators [18–20] that exhibit the quantum spin Hall effect [21–24]. Very recently, the non-quantized intrinsic spin Hall effect [25–28] has been realized experimentally in a quantum gas [29], and the authors of this paper outline the way forward to reaching conditions where the quantum spin Hall effect could be observed. Furthermore, newly demonstrated methods to simulate strong-enough magnetic fields to probe ultra-cold atom gases in the ordinary quantum-Hall regime [30, 31] are expected to be adaptable for the purpose of generating spin-dependent quantizing magnetic fields [30, 32], which opens up another avenue towards the exploration of quantum-spin-Hall physics. Part of the motivation for our present theoretical work arises from these rapid developments of experimental capabilities.

The ordinary quantum Hall (QH) effect [33] occurs because particles confined to move in two spatial dimensions and subject to a strong perpendicular magnetic field develop incompressibilities at integer, and certain fractional, values of the Landau-level filling factor [34]. While the Landau quantization of single-particle energies is the origin of the integer QH effect, incompressibility at fractional filling factors is caused by the discrete spectrum of interaction energies for two particles occupying states from the same Landau level [35–37]. In the conceptually simplest realization of the quantum *spin* Hall (QSH) effect [22], particles exhibit an integer QH effect due to a spin-dependent perpendicular magnetic field that points in opposite directions for the two opposite-spin components. It seems then quite straightforward to conjecture [22, 38] that a fractional version of the QSH effect should exist that mirrors features of the ordinary fractional QH effect in multi-component systems [39–41]. Following this line of thought, some previous discussions of a putative fractional QSH physics [38, 42] have been based on an *ad hoc* adaptation of trial wave functions first proposed in Ref. [22]. However, unless only particles with the same spin interact, such an approach is fraught with difficulty [43].

Here we revisit the question of how a fractional QSH effect can arise in an interacting (pseudo-)spin-1/2 system that experiences a spin-dependent quantizing magnetic field. In particular, we elucidate the effect of interactions between particles having opposite spin. We find that such inter-species interactions significantly alter the expected

QSH physics, but they also open up new opportunities for tailoring the properties of quantum many-particle states. Our study is complementary to recent investigations of fractional QSH phases [43–47] that arise in materials with exotic topological band structures [48–51] or strained graphene [52]. The results obtained here are relevant for electronic systems as well as for ultra-cold bosonic or fermionic atoms. Particular attention is paid to trapped bosons.

The article is organized as follows. In Sec. 2, we introduce the basic model description of an interacting system of (pseudo-)spin-1/2 particles that are subject to a spin-dependent magnetic field. The single-particle states are given in the representation of spin-dependent guiding-center and Landau-level quantum numbers. The eigenvalue problem of two interacting particles is solved – for both cases of equal and opposite-spin particles – in the subsequent Sec. 3. When the two interacting particles have opposite spin, important differences arise with respect to the classic results obtained [53] for spinless (or same-spin) particles. We explore the ramifications of this fact by numerical exact-diagonalization studies with up to 6 bosons for which results are presented in Sec. 4. Our conclusions are summarized in Sec. 5.

2. Pseudo-spin-1/2 particles subject to a spin-dependent magnetic field

We consider a gas of particles (e.g., atoms) that carry a (pseudo-)spin-1/2 degree of freedom and are confined to move in the xy plane. A spin-dependent vector potential

$$\mathcal{A}(\mathbf{r}) = \frac{\mathcal{B}}{2} (-y \hat{\mathbf{x}} + x \hat{\mathbf{y}}) \sigma_z \equiv \begin{pmatrix} \mathcal{A}^{(+)}(\mathbf{r}) & 0 \\ 0 & \mathcal{A}^{(-)}(\mathbf{r}) \end{pmatrix} \quad (1)$$

is presumed to be generated (e.g., by optical means in an atom gas [4, 29, 30, 32]). Here σ_z denotes the diagonal Pauli matrix, and the $\hat{\mathbf{j}}$ are Cartesian unit vectors in real space.

The vector potential (1) is Abelian and gives rise to a spin-dependent magnetic field perpendicular to the xy plane: $\mathcal{B} \equiv \nabla \times \mathcal{A} = \mathcal{B} \hat{\mathbf{z}} \sigma_z$. This situation of opposite-spin particles being subjected to oppositely directed magnetic fields corresponds directly to setups considered for a semiconductor heterostructure [22, 54] and in neutral-atom systems [27–29, 32]. A somewhat related study in the context of cold bosonic gases was given in Ref. [55], only that there the two spin components also experience a large Zeeman-like energy shift and, therefore, this work focused only on the dynamics of a single component.

Without loss of generality, we will assume $\mathcal{B} > 0$ from now on. Also note that, with unit conventions chosen in this article, the ‘magnetic-field’ magnitude \mathcal{B} is related to a fundamental (‘magnetic’) length scale $l_{\mathcal{B}} = \sqrt{\hbar/\mathcal{B}}$.

2.1. Many-particle model Hamiltonian

The most general form of the many-body Hamiltonian that describes our system of interest is $\mathcal{H} = \mathcal{H}_0 + \mathcal{H}_{\text{int}}$, where

$$\mathcal{H}_0 = \int d^2r \hat{\Psi}^\dagger(\mathbf{r}) \left\{ \frac{1}{2M} [\mathbf{p} \hat{1} - \mathcal{A}(\mathbf{r})]^2 + \mathcal{V}(\mathbf{r}) - \mu \hat{1} \right\} \hat{\Psi}(\mathbf{r}) \quad , \quad (2a)$$

$$\mathcal{H}_{\text{int}} = \int d^2r \sum_{\sigma, \sigma' = \pm} \frac{g_{\sigma\sigma'}}{2} \hat{\Psi}_\sigma^\dagger(\mathbf{r}) \hat{\Psi}_{\sigma'}^\dagger(\mathbf{r}) \hat{\Psi}_{\sigma'}(\mathbf{r}) \hat{\Psi}_\sigma(\mathbf{r}) \quad . \quad (2b)$$

Here $\hat{1}$ denotes the 2×2 unit matrix, and $\hat{\Psi}(\mathbf{r}) \equiv \left(\hat{\Psi}_+(\mathbf{r}), \hat{\Psi}_-(\mathbf{r}) \right)^T$ is a two-spinor of (bosonic or fermionic) annihilation operators for a particle located at position \mathbf{r} and having a definite pseudo-spin-1/2 projection along the $\hat{\mathbf{z}}$ axis. Furthermore, the relation $g_{+-} = g_{-+}$ is implicit in the formalism. As it is often useful, we also give an equivalent expression for the interaction part of the Hamiltonian,

$$\mathcal{H}_{\text{int}} = \mathcal{H}_{\text{int}}^{(0)} + \mathcal{H}_{\text{int}}^{(1)} + \mathcal{H}_{\text{int}}^{(2)} \quad , \quad (3a)$$

$$\mathcal{H}_{\text{int}}^{(0)} = \frac{g_0}{2} \int d^2r \sum_{\sigma} \hat{\Psi}_\sigma^\dagger \left(\hat{\Psi}^\dagger \hat{\Psi} \right) \hat{\Psi}_\sigma \quad , \quad (3b)$$

$$\mathcal{H}_{\text{int}}^{(1)} = \frac{g_1}{2} \int d^2r \sum_{\sigma} \sigma \hat{\Psi}_\sigma^\dagger \hat{\Psi}_\sigma^\dagger \hat{\Psi}_\sigma \hat{\Psi}_\sigma \quad , \quad (3c)$$

$$\mathcal{H}_{\text{int}}^{(2)} = \frac{g_2}{2} \int d^2r \sum_{\sigma} \sigma \hat{\Psi}_\sigma^\dagger \left(\hat{\Psi}^\dagger \sigma_z \hat{\Psi} \right) \hat{\Psi}_\sigma \quad , \quad (3d)$$

with $g_0 = \sum_{\sigma\sigma'} g_{\sigma\sigma'}/4$, $g_1 = (g_{++} - g_{--})/2$, and $g_2 = (g_{++} + g_{--} - 2g_{+-})/4$. Depending on whether the asymmetric interaction couplings g_1 , g_2 are positive or negative, different physical regimes may be reached [56, 57].[‡]

In the case where $g_{+-} = 0$, the system reduces to two independent two-dimensional (electron or atom) gases that are each subject to a perpendicular magnetic field. Known phenomena associated with the fractional QH effect [33, 34, 36, 37] will then be exhibited by the individual systems. However, as seen from our study presented in Secs. 3 and 4 below, the behavior of the system with $g_{+-} \neq 0$ departs from the previously considered [39] two-component fractional-QH physics because of the very different type of constraints that is placed on the orbital motion of particles subject to oppositely directed magnetic fields.

2.2. Spin-dependent single-particle Landau levels

We now consider single-particle states associated with spin component σ . The kinetic momentum is $\boldsymbol{\pi}^{(\sigma)} = \mathbf{p} - \mathcal{A}^{(\sigma)}$, and straightforward calculation establishes the

[‡] The notation used in Eqs. (3b)–(3d) can be related to that which is often adopted in the atom-gas literature [58, 59] by setting $g_0 \equiv c_0$, $g_2 \equiv c_2$, and $g_1 \equiv 0$. See also Ref. [60]. Note, however, the different parameterization used in Ref. [8] where $c_{0,2}$ are interaction constants associated with the atomic spin-1 degree of freedom from which the pseudo-spin-1/2 components are derived. Our notation is related to theirs via $g_0 \equiv c_0 + \frac{3}{4}c_2 + \frac{1}{4}c'_{\uparrow\downarrow}$, $g_1 \equiv -\frac{1}{2}c_2$, and $g_2 \equiv -\frac{1}{4}(c_2 + c'_{\uparrow\downarrow})$.

commutation relations

$$[\pi_{\alpha}^{(\sigma)}, \pi_{\alpha'}^{(\sigma')}] = \sigma i \frac{\hbar^2}{l_B^2} \delta_{\sigma\sigma'} \epsilon_{\alpha\alpha'} \quad , \quad (4)$$

where $\epsilon_{xy} = -\epsilon_{yx} = 1$. Operators for the guiding-center locations can then be defined in the usual manner [34], $\mathbf{R}^{(\sigma)} = \mathbf{r} - \sigma l_B^2 [\hat{\mathbf{z}} \times \boldsymbol{\pi}^{(\sigma)}]/\hbar$, and their components satisfy the commutation relations

$$[R_{\alpha}^{(\sigma)}, R_{\alpha'}^{(\sigma')}] = -\sigma i l_B^2 \delta_{\sigma\sigma'} \epsilon_{\alpha\alpha'} \quad . \quad (5)$$

Moreover, we find $[R_{\alpha}^{(\sigma)}, \pi_{\alpha'}^{(\sigma')}] = 0$. Following the familiar approach [34], we define the harmonic-oscillator Landau-level ladder operator for states with spin σ via

$$a_{\sigma} = \frac{i l_B}{\sqrt{2} \hbar} (\pi_x^{(\sigma)} + \sigma i \pi_y^{(\sigma)}) \quad . \quad (6)$$

Similarly, the ladder operator operating within a Landau level for spin component σ is

$$b_{\sigma} = \frac{1}{\sqrt{2} l_B} (R_x^{(\sigma)} - \sigma i R_y^{(\sigma)}) \quad . \quad (7)$$

We can express the kinetic energy and the z component of angular momentum in terms of the ladder operators [$\omega_c = \hbar/(Ml_B^2)$]:

$$\frac{[\boldsymbol{\pi}^{(\sigma)}]^2}{2M} = \hbar\omega_c \left(a_{\sigma}^{\dagger} a_{\sigma} + \frac{1}{2} \right) \quad , \quad (8a)$$

$$L_z \equiv x p_y - y p_x = \hbar \sigma (b_{\sigma}^{\dagger} b_{\sigma} - a_{\sigma}^{\dagger} a_{\sigma}) \quad . \quad (8b)$$

Landau-level eigenstates are generated via

$$|\{n_{\sigma}, m_{\sigma}\}\rangle = \left[\sum_{\sigma} \frac{(a_{\sigma}^{\dagger})^{n_{\sigma}}}{\sqrt{n_{\sigma}!}} \frac{(b_{\sigma}^{\dagger})^{m_{\sigma}}}{\sqrt{m_{\sigma}!}} \mathcal{P}_{\sigma} \right] |\text{vac}\rangle \quad , \quad (9)$$

where $|\text{vac}\rangle = (1, 1)^T |0\rangle$ and $|0\rangle$ is the state that is annihilated by all ladder operators a_{σ} and b_{σ} . In the following, we will focus on the case where all particles are in the lowest Landau level, i.e., when $n_{+} = n_{-} = 0$.

3. Two-particle interactions in the lowest Landau level: Spin matters

3.1. Heuristic real-space picture

Before presenting a formal analysis of the interacting two-particle system subject to a strong spin-dependent magnetic field in the following Subsection, we provide a heuristic argument for how the cases where the two particles feel the same and opposite magnetic fields differ.

Consider two particles, located at \mathbf{r}_1 and \mathbf{r}_2 , respectively, that interact via a generic potential $V(\mathbf{r}_1 - \mathbf{r}_2)$. The corresponding first-quantized two-particle Hamiltonian reads

$$\mathcal{H}_{1,2} = \frac{[\mathbf{p}_1 - \mathcal{A}^{(\sigma_1)}(\mathbf{r}_1)]^2}{2M} + \frac{[\mathbf{p}_2 - \mathcal{A}^{(\sigma_2)}(\mathbf{r}_2)]^2}{2M} + V(\mathbf{r}_1 - \mathbf{r}_2) \quad , \quad (10)$$

with the spin-dependent vector potentials from Eq. (1). It is straightforward to show that the sum of kinetic-energy contributions for each particle can be re-arranged in terms of the linear combinations

$$\mathbf{R}_{\sigma_1\sigma_2} = \frac{1}{2} \begin{pmatrix} x_1 + x_2 \\ y_1 + \sigma_1\sigma_2 y_2 \end{pmatrix}, \quad \mathbf{r}_{\sigma_1\sigma_2} = \frac{1}{2} \begin{pmatrix} x_1 - x_2 \\ y_1 - \sigma_1\sigma_2 y_2 \end{pmatrix}, \quad (11)$$

yielding the expression

$$\mathcal{H}_{1,2} = \frac{[\mathbf{P}_{\sigma_1\sigma_2} - 2\mathcal{A}^{(+)}(\mathbf{R}_{\sigma_1\sigma_2})]^2}{2M} + \frac{[\mathbf{p}_{\sigma_1\sigma_2} - 2\mathcal{A}^{(+)}(\mathbf{r}_{\sigma_1\sigma_2})]^2}{2M} + V(\mathbf{r}_1 - \mathbf{r}_2). \quad (12)$$

The two-particle problem for particles with the same spin reduces to two independent single-particle problems in the center-of-mass (COM) and relative-coordinate degrees of freedom ($\mathbf{R}_{\sigma\sigma}$ and $\mathbf{r}_{\sigma\sigma}$, respectively) because $\mathbf{r}_1 - \mathbf{r}_2 \equiv 2\mathbf{r}_{\sigma\sigma}$. In that case, only the relative-coordinate degree of freedom feels the interaction potential $V(\mathbf{r}_{\sigma\sigma})$, and it can be minimized by placing two particles away from each other. In the specific case of $V(\mathbf{r}) \propto \delta(\mathbf{r})$, the zero-energy states of the two-particle system are of the form $\psi_{\sigma\sigma}(\mathbf{r}_1, \mathbf{r}_2) \propto (z_1 + z_2)^{m_C} (z_1 - z_2)^{m_r}$, where $z_j = x_j + i y_j$ is a commonly used complex notation for the position of particle j [34]. The non-negative integers m_C and m_r correspond to the quantized values of COM angular momentum and relative angular momentum, respectively [34].

Quite a different situation arises for opposite-spin particles. The kinetic energy of the two-particle system decouples in the coordinates \mathbf{R}_{+-} and \mathbf{r}_{+-} , motivating the proposal of trial wave functions [22] $\psi_{+-}(\mathbf{r}_1, \mathbf{r}_2) \propto (z_1 + z_2^*)^{m_C} (z_1 - z_2^*)^{m_r}$. However, $V(\mathbf{r})$ still couples the two-particle coordinates \mathbf{R}_{+-} and \mathbf{r}_{+-} and, as a result, the proposed wave function is energetically not favorable for interacting particles [43]. Rigorous examination of the interacting two-particle system in the opposite-spin configuration (see below) shows that energy eigenstates are not eigenstates of COM angular momentum or relative angular momentum and, furthermore, have an unusual distribution.

3.2. Rigorous analysis of interaction matrix

To gain a deeper understanding of the effect of two-particle interactions, we follow the basic approach employed by previous studies of the fractional QH effect [34, 35] and find the interaction potential in the representation of lowest-Landau-level states. The starting point of such an analysis is the Fourier decomposition of a spin-dependent interaction potential given by

$$V_{\sigma_1\sigma_2}(\mathbf{r}_1 - \mathbf{r}_2) = \int \frac{d^2q}{(2\pi)^2} V_{\sigma_1\sigma_2}(\mathbf{q}) e^{i\mathbf{q}\cdot(\mathbf{r}_1 - \mathbf{r}_2)}, \quad (13)$$

because its matrix elements can then be directly related to the corresponding matrix elements of the exponential in the integrand of (13). To find the latter for states in the

lowest Landau level, we use the relation

$$\mathbf{r}_1 - \mathbf{r}_2 = \mathbf{R}_1^{(\sigma_1)} - \mathbf{R}_2^{(\sigma_2)} + \frac{l_B^2}{\hbar} \hat{\mathbf{z}} \times \left(\sigma_1 \boldsymbol{\pi}_1^{(\sigma_1)} - \sigma_2 \boldsymbol{\pi}_2^{(\sigma_2)} \right) \quad (14)$$

and the straightforwardly obtained expressions

$$\mathbf{q} \cdot \left(\mathbf{R}_1^{(\sigma_1)} - \mathbf{R}_2^{(\sigma_2)} \right) = \frac{l_B}{\sqrt{2}} \left[q_x (b_{\sigma_1} - b_{\sigma_2} + b_{\sigma_1}^\dagger - b_{\sigma_2}^\dagger) + \sigma_1 i q_y (b_{\sigma_1} - \sigma_1 \sigma_2 b_{\sigma_2} - b_{\sigma_1}^\dagger + \sigma_1 \sigma_2 b_{\sigma_2}^\dagger) \right], \quad (15a)$$

$$\frac{l_B^2}{\hbar} (\mathbf{q} \times \hat{\mathbf{z}}) \cdot \left(\sigma_1 \boldsymbol{\pi}_1^{(\sigma_1)} - \sigma_2 \boldsymbol{\pi}_2^{(\sigma_2)} \right) = \frac{l_B}{\sqrt{2}} \left[q_x (a_{\sigma_1} - a_{\sigma_2} + a_{\sigma_1}^\dagger - a_{\sigma_2}^\dagger) + \sigma_1 i q_y (a_{\sigma_1} - \sigma_1 \sigma_2 a_{\sigma_2} - a_{\sigma_1}^\dagger + \sigma_1 \sigma_2 a_{\sigma_2}^\dagger) \right]. \quad (15b)$$

Introducing spin-resolved ladder operators for COM and relative angular momentum,

$$b_{\sigma_1 \sigma_2}^{(C)} = \frac{b_{1\sigma_1} + b_{2\sigma_2}}{\sqrt{2}}, \quad b_{\sigma_1 \sigma_2}^{(r)} = \frac{b_{1\sigma_1} - b_{2\sigma_2}}{\sqrt{2}}, \quad (16)$$

and analogous ladder operators for COM energy and relative-motion energy,

$$a_{\sigma_1 \sigma_2}^{(C)} = \frac{a_{1\sigma_1} + a_{2\sigma_2}}{\sqrt{2}}, \quad a_{\sigma_1 \sigma_2}^{(r)} = \frac{a_{1\sigma_1} - a_{2\sigma_2}}{\sqrt{2}}, \quad (17)$$

we find using $q_\sigma = q_x + \sigma i q_y$

$$e^{i\mathbf{q} \cdot (\mathbf{R}_1^{(\sigma_1)} - \mathbf{R}_2^{(\sigma_2)})} = e^{-\frac{q^2 l_B^2}{2}} \times \begin{cases} e^{i\bar{q}_\sigma l_B b_{\sigma\sigma}^{(r)\dagger}} e^{iq_\sigma l_B b_{\sigma\sigma}^{(r)}} & \text{for } \sigma_1 = \sigma_2 \equiv \sigma \\ e^{iq_x l_B b_{\sigma,-\sigma}^{(r)\dagger}} e^{iq_x l_B b_{\sigma,-\sigma}^{(r)}} e^{\sigma q_y l_B b_{\sigma,-\sigma}^{(C)\dagger}} e^{-\sigma q_y l_B b_{\sigma,-\sigma}^{(C)}} & \text{for } \sigma_1 = -\sigma_2 \equiv \sigma \end{cases}, \quad (18a)$$

$$e^{i\frac{l_B^2}{\hbar} (\mathbf{q} \times \hat{\mathbf{z}}) \cdot (\sigma_1 \boldsymbol{\pi}_1^{(\sigma_1)} - \sigma_2 \boldsymbol{\pi}_2^{(\sigma_2)})} = e^{-\frac{q^2 l_B^2}{2}} \times \begin{cases} e^{i\bar{q}_\sigma l_B a_{\sigma\sigma}^{(r)\dagger}} e^{iq_\sigma l_B a_{\sigma\sigma}^{(r)}} & \text{for } \sigma_1 = \sigma_2 \equiv \sigma \\ e^{iq_x l_B a_{\sigma,-\sigma}^{(r)\dagger}} e^{iq_x l_B a_{\sigma,-\sigma}^{(r)}} e^{\sigma q_y l_B a_{\sigma,-\sigma}^{(C)\dagger}} e^{-\sigma q_y l_B a_{\sigma,-\sigma}^{(C)}} & \text{for } \sigma_1 = -\sigma_2 \equiv \sigma \end{cases} \quad (18b)$$

Inspection of Eqs. (18a)–(18b) reveals a very important formal difference between cases when the interacting particles have equal or opposite spin. For a pair of particles with the same spin, the interaction only couples to the relative-motion Landau-level degrees of freedom. In contrast, for particles with opposite spin, the interaction involves both the relative-motion *and the COM* degrees of freedom. This latter situation is unlike any other encountered previously in the context of fractional QH physics.

With the expressions (18a)–(18b), we are now able to express the interaction potential for a pair of particles having spin σ_1 and σ_2 , respectively, in the basis of COM-angular-momentum and relative-angular-momentum eigenstates from the lowest Landau level given by

$$|m_C, m_r\rangle_{\sigma_1 \sigma_2} = \frac{[b_{\sigma_1 \sigma_2}^{(C)\dagger}]^{m_C}}{\sqrt{m_C!}} \frac{[b_{\sigma_1 \sigma_2}^{(r)\dagger}]^{m_r}}{\sqrt{m_r!}} |0\rangle_1 \otimes |0\rangle_2. \quad (19)$$

For clarity, the cases where the interacting particles have equal or opposite spin will be discussed separately.

3.2.1. Interaction of particles with same spin The fact that only the relative-angular-momentum operators enter the expression (18a) for $\sigma_1 = \sigma_2 \equiv \sigma$ implies that the interaction matrix is diagonal in COM space. Straightforward calculation yields

$$\sigma\sigma \langle m_C, m_r | e^{i\mathbf{q}\cdot(\mathbf{r}_1 - \mathbf{r}_2)} | m'_C, m'_r \rangle_{\sigma\sigma} = \delta_{m_C m'_C} e^{-q^2 l_B^2} \mathcal{M}_{m_r m'_r}(q_\sigma l_B), \quad (20)$$

where

$$\mathcal{M}_{mm'}(\kappa) = \left(\frac{m!}{m'!} \right)^{1/2} (i\kappa)^{m'-m} L_m^{m'-m}(|\kappa|^2) \quad (21)$$

in terms of the generalized Laguerre polynomial $L_m^{m'-m}$. Using the result (20) and the relation (13) for a contact interaction where $V_{\sigma_1\sigma_2}(\mathbf{q}) = g_{\sigma_1\sigma_2}$ yields the well-known expression [34–36]

$$\sigma\sigma \langle m_C, m_r | V_{\sigma\sigma}(\mathbf{r}_1 - \mathbf{r}_2) | m'_C, m'_r \rangle_{\sigma\sigma} = \frac{g_{\sigma\sigma}}{4\pi l_B^2} \delta_{m_C m'_C} \delta_{m_r m'_r} \delta_{m_r 0} \quad (22)$$

for the interaction matrix elements. The remarkable result (22) underpins the basic description of fractional-QH physics [34,36]. It implies that the two-particle eigenstates are also eigenstates of COM and relative angular momentum. Furthermore, the energy spectrum of two particles with spin σ from the lowest Landau level is two-valued: states with $m_r = 0$ and arbitrary m_C have energy $\hbar\omega_c + g_{\sigma\sigma}/(4\pi l_B^2)$, and all other states have energy $\hbar\omega_c$.

3.2.2. Interaction of particles with opposite spin Using (18a) for the case $\sigma_1 = -\sigma_2 \equiv \sigma$, we find

$$\begin{aligned} \sigma, -\sigma \langle m_C, m_r | e^{i\mathbf{q}\cdot(\mathbf{r}_1 - \mathbf{r}_2)} | m'_C, m'_r \rangle_{\sigma, -\sigma} &= e^{-q^2 l_B^2} \\ &\times (i\sigma)^{m'_C - m_C} \mathcal{M}_{m_r m'_r}(q_x l_B) \mathcal{M}_{m_C m'_C}(q_y l_B). \end{aligned} \quad (23)$$

The contact-interaction matrix element for opposite-spin particles is then calculated as

$$\begin{aligned} \sigma, -\sigma \langle m_C, m_r | V_{\sigma, -\sigma}(\mathbf{r}_1 - \mathbf{r}_2) | m'_C, m'_r \rangle_{\sigma, -\sigma} \\ = \frac{g_{+-}}{(2\pi l_B)^2} i^{m'_r - m_r} \mathcal{R}_{m_r m'_r} \mathcal{R}_{m_C m'_C}, \end{aligned} \quad (24)$$

with

$$\mathcal{R}_{mm'} = \frac{[1 + (-1)^{m'-m}]}{2\sqrt{m! m'!}} \Gamma\left(\frac{m + m' + 1}{2}\right) \quad (25)$$

in terms of the Euler Gamma function $\Gamma(x)$. Thus we find that the interaction matrix for two particles from the lowest Landau level with opposite spin is nondiagonal in the COM-angular-momentum and relative-angular-momentum spaces. This is markedly different from the case of same-spin particles.

Straightforward diagonalization of the matrix (24) yields the two-particle eigenenergies E_n when both particles have opposite spin. Figure 1A shows a logarithmic plot of the E_n , ordered by decreasing magnitude, for different values m_{\max} of the cut-off value for COM and relative angular momentum. We observe an exponential dependence

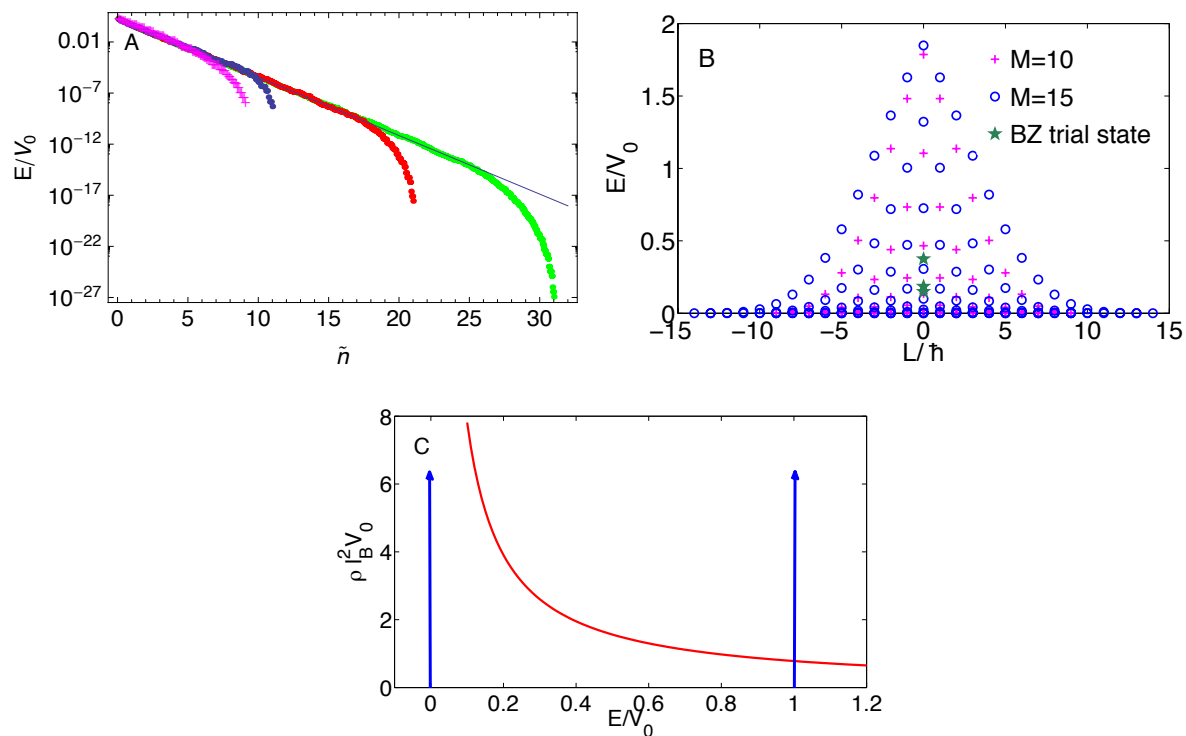


Figure 1. Panel A: Eigenvalues E of the opposite-spin two-particle interaction matrix [cf. Eq. (24)] in units of $V_0 \equiv g_{+-}/(4\pi l_B^2)$, sorted by magnitude. Data are shown for various values of the angular-momentum cutoff $m_{\max} = 10$ (blue), 20 (red), 30 (green), and $\tilde{n} = n/(m_{\max} + 1)$. The straight line is a plot of $E = 0.3 V_0 \exp(-\alpha \tilde{n})$ with $\alpha = 1.28$. Panel B: Energy spectrum obtained for a system of two particles with opposite spin by exact diagonalization. A finite system size is imposed by limiting the number of modes available in angular-momentum space for each particle to \mathcal{M} . Note the \mathcal{M} -dependence of the obtained values. The data for $\mathcal{M} = 10$ are also shown as the magenta data points in panel A and exhibit excellent agreement with the power-law-type distribution predicted from the solution in COM and relative angular-momentum space. Green stars show the energy calculated for two-particle versions of trial states [22] $\psi_{+-}(\mathbf{r}_1, \mathbf{r}_2) \propto (z_1 + z_2^*)^{m_C} (z_1 - z_2^*)^{m_r}$ with $m_C = 0$ and $m_r = 2, 9, 14$. Higher m_r is observed to correlate with lower energy, but there are many states even lower in energy than the trial state with largest m_r that is compatible with the finite systems size. Panel C: Comparison of two-particle densities of states for same-spin case (blue arrows indicating delta functions) and for opposite-spin case (red curve).

of the sorted eigenvalues as a function of the scaled index $\tilde{n} = n/(m_{\max} + 1)$, which translates into a power-law density of states

$$\rho(E) = \left| \frac{\Delta n}{\Delta A \Delta E} \right| \approx \frac{1}{\alpha l_B^2 E} \quad (26)$$

Here $\Delta A = (m_{\max} + 1)l_B^2$ is the area corresponding to the cut-off in COM and relative angular momentum, and $\alpha \approx 1.28$ has been determined numerically. The numerical data deviate from Eq. (26) close to the maximum energy $g_{+-}/(2\pi l_B^2)$, where the density of states reaches zero, and for small energy where it becomes cutoff dependent. None

of the individual eigenvalues is strictly independent of the cutoff, which indicates that there are no compact eigenstates. Figure 1C illustrates the different density-of-states behavior for interacting two-particle systems for the two cases of particles having the same and opposite spin, respectively.

It is also useful to look at the distribution of eigenvalues over total angular momentum. We do this with a different numerical scheme using exact diagonalization of the two-particle Hilbert space on a disk, as it preserves the z component of angular momentum as a good quantum number. (Details are given in the following section.) The spectrum for $N_+ = N_- = 1$ is shown in Fig. 1B. Note the dependence of the eigenvalues on the systems size (ie, the cut-off in angular momentum of available Landau-level states). Any systematic difference between the results given in Figs. 1A and 1B is probably at least in part due to the fact that the representation using the COM and relative angular-momentum basis assumes an infinite number of single-particle angular-momentum modes to be available to the particles. Nevertheless, when the energy eigenvalues obtained for the finite system are plotted alongside the results for the analytical model (see magenta data points in Fig. 1A), both are seen to exhibit the same exponential behavior. For comparison, the energies calculated for proposed trial states [22] are also shown in Fig. 1B as green stars.

4. Few-particle systems studied by numerically exact diagonalization

While the interacting two-particle problem has lent itself to analytical study, the behavior of systems with three or more interacting particles either requires approximate, e.g., variational, approaches or must be done numerically. As the complications encountered already for the case of two interacting particles with opposite spin stymie progress for the variational option, we follow the numerical route here.

4.1. Formalism and results for few-particle eigen-energy spectra

We start by representing the Schrödinger field operator for a particle at position \mathbf{r} with spin σ projected onto the lowest spin-related Landau level,

$$\hat{\Psi}_\sigma^{(\text{LLL})}(\mathbf{r}) = \sum_{m \geq 0} \phi_{0,m}^{(\sigma)}(\mathbf{r}) \hat{c}_{\sigma m} \quad , \quad (27)$$

where $\hat{c}_{\sigma m}^\dagger$ creates a particle in component σ with angular momentum σm in the state $\phi_{0,m}^{(\sigma)}(\mathbf{r}) \equiv \langle \mathbf{r} | (b_\sigma^\dagger)^m / \sqrt{m!} | 0 \rangle$. Substituting this into Eq. (2b), we get

$$\mathcal{H}_{\text{int}}^{(\text{LLL})} = \sum_{\sigma \sigma'} \sum_{\{m\}} \Lambda_{\{m\}}^{(\sigma, \sigma')} \hat{c}_{\sigma m_1}^\dagger \hat{c}_{\sigma' m_2}^\dagger \hat{c}_{\sigma' m_3} \hat{c}_{\sigma m_4} \quad , \quad (28)$$

where

$$\Lambda_{\{m\}}^{(\sigma, \sigma')} = \frac{g_{\sigma \sigma'}}{2} \int d^2 r \left[\phi_{0,m_1}^{(\sigma)}(\mathbf{r}) \right]^* \left[\phi_{0,m_2}^{(\sigma')}(\mathbf{r}) \right]^* \phi_{0,m_3}^{(\sigma')}(\mathbf{r}) \phi_{0,m_4}^{(\sigma)}(\mathbf{r}) \quad . \quad (29)$$

For same-spin particles, i.e., $\sigma' = \sigma$, we obtain

$$\Lambda_{\{m\}}^{(\sigma,\sigma)} = \frac{g_{\sigma\sigma}}{8\pi l_B^2} \frac{(m_1 + m_2)! \delta_{m_1+m_2, m_3+m_4}}{2^{m_1+m_2} \sqrt{m_1! m_2! m_3! m_4!}}. \quad (30)$$

In contrast, for the matrix element involving opposite-spin particles ($\sigma = -\sigma'$), we find

$$\Lambda_{\{m\}}^{(\sigma,-\sigma)} = \frac{g_{\sigma,-\sigma}}{8\pi l_B^2} \frac{(m_1 + m_3)! \delta_{m_1+m_3, m_2+m_4}}{2^{m_1+m_3} \sqrt{m_1! m_2! m_3! m_4!}}. \quad (31)$$

The way indices are distributed in the arguments of the δ -functions in Eqs. (30) and (31) implies that the system's total angular momentum $L \equiv \sum_j L_{zj}$ [cf. Eq. (8b) for the definition of L_z] is a conserved quantity in the presence of interactions.

Cold-atom systems are usually studied while trapped by an external potential of tunable strength. To model this situation, we introduce the second-quantized form of a parabolic potential in the representation of lowest-Landau-level states,

$$\mathcal{H}_0^{(\text{LLL})} = \sum_{\sigma, m} \alpha(m+1) \hat{c}_{\sigma m}^\dagger \hat{c}_{\sigma m}, \quad (32)$$

where $\alpha = M\Omega^2 l_B^2$ in terms of the harmonic-trap frequency Ω . Switching on the trap will lift degeneracies of few-particle states and serve to identify the most compact ground states of our systems of interest.

We calculate the few-particle energy spectra and associated eigenstates for $\mathcal{H}_0^{(\text{LLL})} + \mathcal{H}_{\text{int}}^{(\text{LLL})}$ in the Fock basis of lowest-Landau-level states for the two spin components. We focus here on the case of bosonic particles to be directly applicable to currently studied ultra-cold atom systems, but our general conclusions apply to systems of fermionic particles as well. Results obtained for systems with $N_+ + N_- = 4$ are shown in Fig. 2. Panel A shows the situation where only particles from a single component are present, which is analogous to the previously considered case of spinless bosons [37, 61–63]. The zero-energy state at lowest total angular momentum has $|L| = N(N-1)$ and corresponds to the filling-factor-1/2 Laughlin state [36, 37]. Zero-energy eigenstates at higher magnitudes of total angular momentum correspond to edge excitations of the Laughlin state [34]. The $L = 0$ state has an energy of $V_0 N(N-1)/2$, where $V_0 \equiv g_{++}/(4\pi l_B^2)$.

When particles occupy states in both components, the situation becomes complex. Without interaction between the different spin species, states of each component will be the ones that are obtained by diagonalising the interacting Hamiltonian within that component. The entire system is then essentially an independent superposition of eigenstates for the individual spin species. However, in contrast to ordinary multi-component QH states discussed, e.g., in Refs. [39–41], the total angular momenta for states from different components have opposite sign. Therefore, e.g., the combination of Laughlin states in each component with the same number of particles has zero total angular momentum. This case is illustrated in Fig. 2B. However, the superpositions of edge excitations with same magnitude of excess angular momentum for the opposite-spin Laughlin states will also be zero-energy, zero-angular-momentum eigenstates. To reveal the associated degeneracies of the spectrum shown in Fig. 2B, we obtained the energy

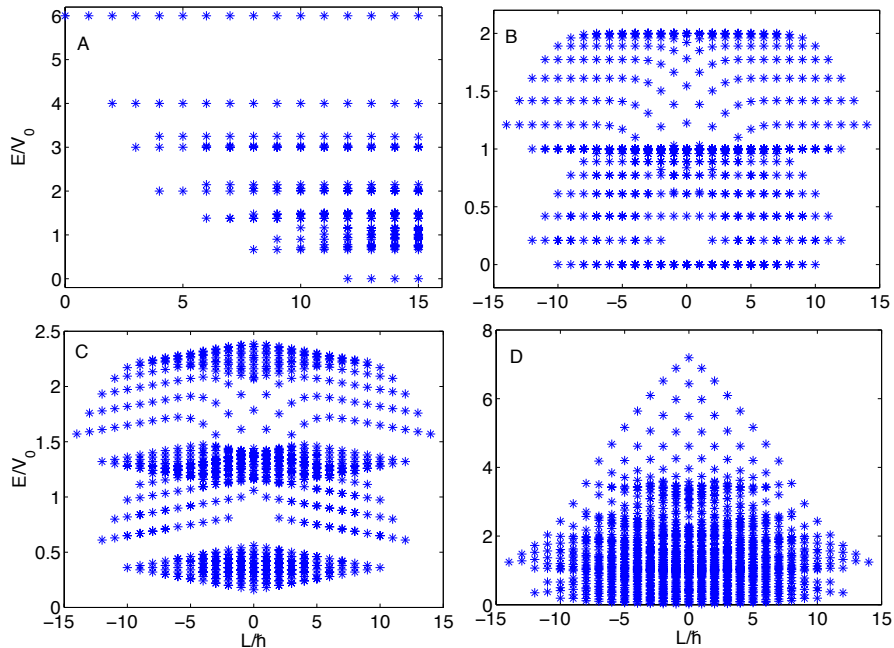


Figure 2. Spectrum for various four-particle systems (i.e., $N_+ + N_- = 4$). Energies are given in units of the intra-species Haldane-pseudopotential energy scale $V_0 = g_{++}/(4\pi l_B^2)$. A: Single-component system with $N_+ = 4$, $N_- = 0$. The four-particle Laughlin state is the zero-energy state with the smallest total angular momentum $L = 12$. B: System with $N_+ = N_- = 2$ and $g_{++} = g_{--} \neq 0$, $g_{+-} = 0$ (no interspecies interaction). C: Same situation as for B but with a finite trapping potential ($\alpha = 0.02$) switched on in addition, revealing the energy degeneracies in B. The lowest-energy state is a superposition of two-particle Laughlin states in each component. D: Same situation as for B but with finite interspecies interaction $g_{+-} = g_{++}$ in addition.

eigenvalues in the presence of a parabolic confinement. See Fig. 2C. Notice the band of low-lying energy levels separated by a gap from higher-energy states. The lowest-energy $L = 0$ state is the superposition of the two-particle Laughlin states for the two spin species. The other states in the low-energy band correspond to edge excitations of this configuration.

Figure 2D illustrates the dramatic effect of interactions between opposite-spin particles. The spectrum seen there has to be compared with that given in panel B where only particles with the same spin interact. Note the disappearance of energy gaps and accumulation of states at low energy, reflecting the characteristic features of the opposite-spin two-particle interaction spectrum shown in Fig. 1B. Clearly, the system is not incompressible anymore, and no QH-related physics can be expected to occur.

In Figure 3, the interplay between interactions and confinement is elucidated. Panels A–D show the evolution of low-lying few-particle eigenstates as the confinement strength is varied for situations with different magnitude of interaction strength between opposite-spin particles. Panel A corresponds to the case with $g_{+-} = 0$. Due to the

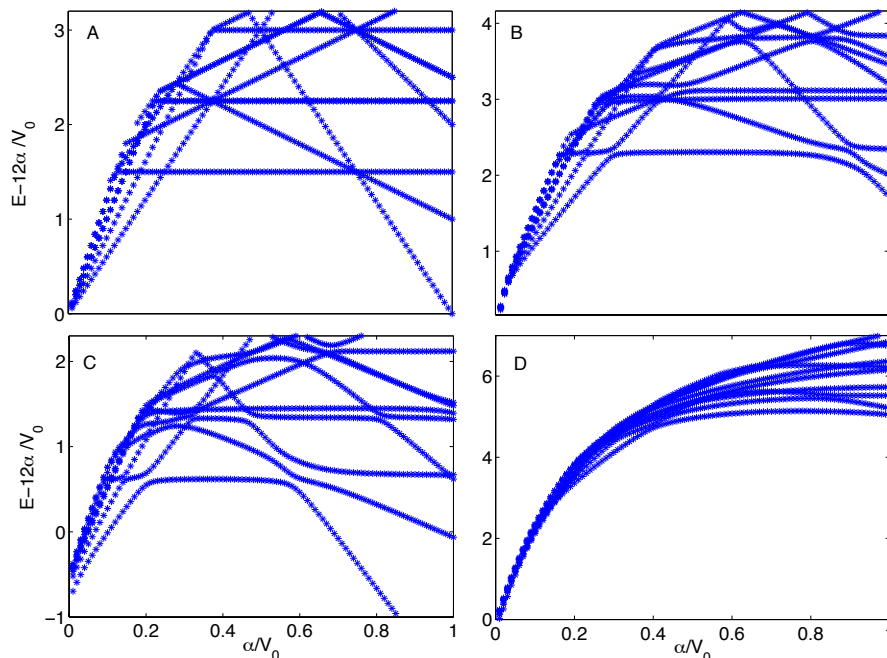


Figure 3. Low-lying energy levels for a system with $N_+ = N_- = 3$ in the sector of total angular momentum $L = 0$. In the calculation, lowest-Landau-level states with $m \leq 18$ have been included. Different panels correspond to different interspecies-interaction strengths. A: No inter-species interactions ($g_{+-} = 0$). A finite trapping potential lifts the energy degeneracies seen at $\alpha = 0$ and singles out a unique lowest-energy state. For small α , the latter turns out to be the superposition of Laughlin states for each individual component. At $\alpha = 0.2$ it becomes an incompressible state with a single Laughlin quasi-particle in each component. Finally, at $\alpha = 0.8$ both components are Bose-condensed in the lowest Landau level. Modest interspecies-interaction strengths ($g_{\sigma\bar{\sigma}} = 0.2 V_0$ in panel B and $g_{\sigma\bar{\sigma}} = -0.2 V_0$ in panel C) cause avoided crossings but preserve the incompressible nature of the states seen in panel A. A stronger interspecies interaction ($g_{+-} = V_0$ in panel D) washes out that picture completely.

occurrence of level crossings, the character of the lowest-energy (ground) state is found to be different for regimes associated with weak, intermediate, and strong confinement. Analogous behavior has been discussed previously for ordinary (spinless) few-boson fractional QH systems [64]. In our case depicted in Fig. 3A, the ground state in the weak-confinement regime corresponds to a superposition of three-particle Laughlin states for filling factor $1/2$ in the individual pseudospin components. After the first level crossing, each component turns out to be in the Laughlin-quasiparticle state [64] and, after another level crossing, each spin component has its three particles occupying the lowest state defined by the parabolic confinement potential. (Our description of the ground states found in the three different regimes is supported by the analysis of real-space density and angular-momentum distribution functions. See the following subsection for details.)

Switching on interactions between opposite-spin particles turns crossings into anti-crossings. Figures. 3B and 3C depict situations where interactions between same-spin particles are still dominant. The existence of anticrossings enables smooth transitions between the different ground states that would not be possible in the case of simple crossings as seen, e.g., in panel A. Independent tuning of interactions between opposite-spin particles can therefore be used to enable engineering of quantum many-particle states in ways not anticipated in previous work [64].

Strong interactions between opposite-spin particles are again seen to fundamentally alter the character of the system's ground and excited states. In Fig. 3D, the strengths of interactions between same-spin and opposite-spin particles are equal. The variation of few-particle states as a function of confinement strength is seen to be almost uniform, again pointing to the loss of distinctiveness for few-particle states in the presence of inter-species interactions. Furthermore, energy differences between low-lying states are much reduced as compared to the situation depicted in panel A of the same figure, which is a reflection of the unusual distribution of energy eigenvalues found for the interacting opposite-spin two-particle system.

4.2. Results for physical properties of the few-particle ground state

The one-particle density profiles in coordinate space and in angular-momentum space are useful quantities to enable greater understanding of the properties of specific many-body quantum states [65, 66]. In the basis of lowest-Landau-level states from the two spin components, the single-particle density matrix of a many-particle state $|\Phi\rangle$ has matrix elements

$$\rho_{\sigma m, \sigma' m'} = \langle \Phi | \hat{c}_{\sigma m}^\dagger \hat{c}_{\sigma' m'} | \Phi \rangle \quad . \quad (33)$$

In terms of this quantity, we can define the angular-momentum distribution for each spin component,

$$\rho_m^{(\sigma)} = \rho_{\sigma m, \sigma m} \quad , \quad (34)$$

and also the spin-resolved single-particle density profile in real space,

$$n^{(\sigma)}(\mathbf{r}) = \sum_{m, m'} \rho_{\sigma m, \sigma m'} \left[\phi_{0, m}^{(\sigma)}(\mathbf{r}) \right]^* \phi_{0, m'}^{(\sigma)}(\mathbf{r}) \quad . \quad (35)$$

In the following, we focus on the properties of the lowest-energy (ground) state in the different regimes associated with small, intermediate, and strong confinement strength for the systems whose energy spectra are shown in Fig. 3.

Figure 4 shows the real-space profile of $n^{(+)}(\mathbf{r})$ across a diameter of the disk-shaped three-particle systems associated with the ground-state levels shown in Fig. 3. In the absence of interactions between opposite-spin particles, each component realizes correlated few-particle states of the type that have been found in previous work [64]. The few-particle filling-factor-1/2 FQH state is the ground state for a weak confinement potential. Increasing the trapping-potential strength favors more compact correlated states, hence, at a critical value of α , a transition occurs to a three-particle version of

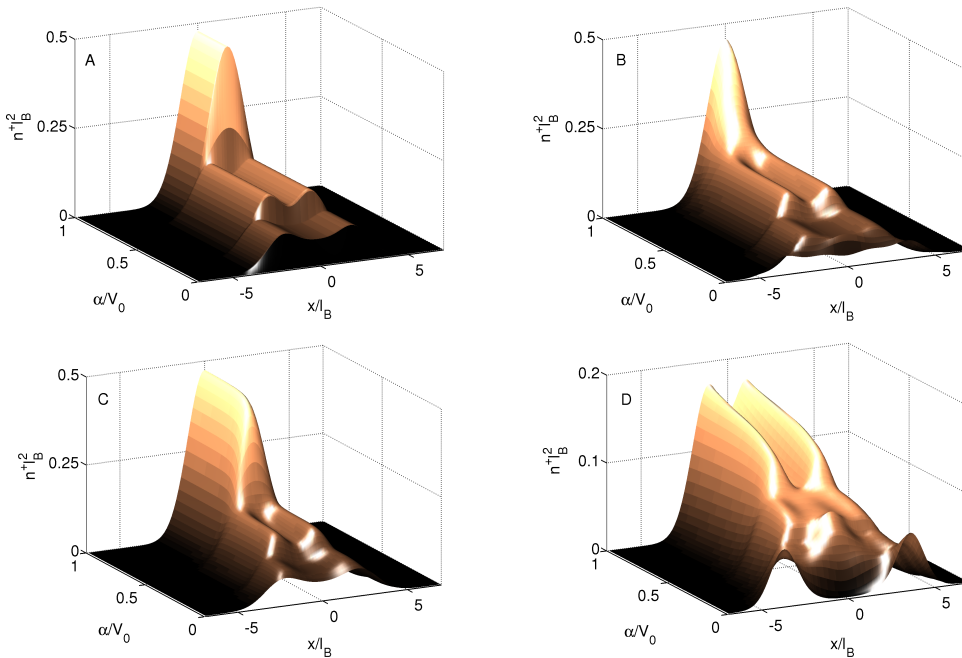


Figure 4. Cross-sectional pseudo-spin + density profiles of the few-particle ground state associated with the lowest-lying energy level shown in the corresponding panels A–D of Fig. 3, aggregated as a function of the confinement-potential strength α . In panel A (only particles with same spin interact), sharp transitions occur between the FQH (Laughlin) state in the regime of small α , a Laughlin-quasiparticle-type state for intermediate α , and the Gaussian Bose-Einstein-condensed state at high α . For moderate interaction strength between opposite-spin components (repulsive in panel B, attractive in panel C), transitions become smooth crossovers associated with anticrossings in Fig. 3. Stronger interactions strengths between the spin components significantly change the character of the few-particle state at small α (panel D).

the Laughlin-quasiparticle excited state. At even higher α , the system transitions to the Gaussian Bose-Einstein-condensate state. The sharpness of the transitions reflects the existence of level crossings in Fig. 3A. Practically, simple variation of α would not lead to any such transitions because there is no mechanism for the system to switch between different many-particle states. To make adiabatic passage between different many-particle states possible, some symmetry of the system needs to be broken, and previous work has proposed scenarios for achieving this in the single-component case [64].

For our system of interest, an additional possibility arises from the ability to tune the interaction strength between the two spin components. As seen in panels B and C of Fig. 3, a moderate value of g_{+-} turns the crossings occurring in panel A into anti-crossings, thus, different many-particle states are now adiabatically connected. Concomitantly, there is a continuous evolution of the spin-resolved one-particle density profile as a function of the confinement strength seen in Figs. 4B and 4C. When interactions between same-spin and opposite-spin particles have the same magnitude, the density profile changes significantly (see Fig. 4D), which indicates that the character

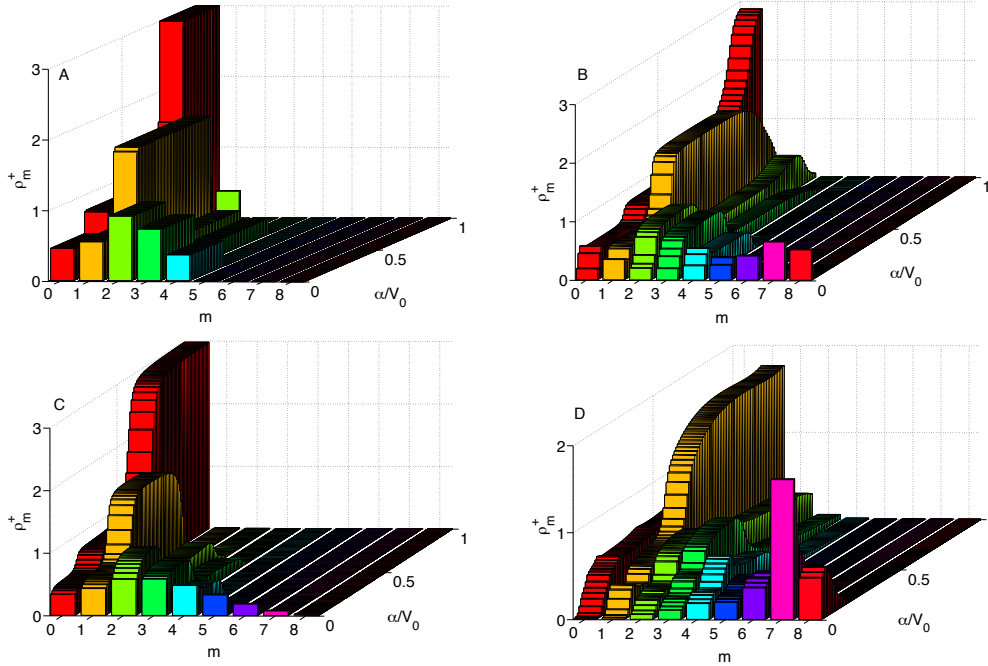


Figure 5. One-particle angular-momentum distribution for pseudo-spin + particles for the ground states of systems whose energy spectra are shown in Fig. 3. Compare also with the real-space density profiles shown in Fig. 4. Note that the single-particle angular momentum cut-off at $m = 10$ defines the sample size for vanishing α in situations where opposite-spin particles interact (panels B – D).

of many-particle ground states is very different from a fractional-QSH state.

Investigation of the one-particle angular-momentum-state distribution for the few-particle ground states discussed so far further solidifies our conclusions. See Figure 5. In the absence of interactions between opposite-spin particles, the characteristic distributions for few-particle versions of the Laughlin and Laughlin-quasiparticle states emerge at low and intermediate values of α . In the limit of strong trapping potential, the system condenses into the $m = 0$ state. Switching on moderate repulsive (attractive) interaction strength between opposite-spin particles smoothens the transitions and also shifts the critical values of α to larger (smaller) values. When interactions among same-spin and between opposite-spin particles have equal magnitude, the one-particle momentum distribution of the ground state differs markedly from that associated with a fractional-QH state. It appears that strong inter-component interactions favor a state with increased occupation of high-angular-momentum states, spreading out the particles more evenly across the accessible sample size and leading to an accumulation at the system's boundary. In the limit of vanishingly small trapping-potential strength α , the latter is defined by the cut-off for single-particle angular momentum applied in our calculations.

5. Conclusions

We have considered the interplay of Landau quantization and spin-dependent interactions in systems where particles with same spin feel the same strong magnetic field whereas particles with opposite spin are subject to magnetic fields with the same magnitude but opposite direction. It has been expected [22, 38, 42] that such systems exhibit the fractional QSH effect, but we find that interactions between particles with opposite spin weaken or destroy features associated with fractional-QSH physics. Similar behavior has been seen in numerical studies of lattice realizations of fractional-QSH systems [47]. We have elucidated how behavior that is very different from ordinary two-component fractional-QH systems is rooted in the drastically different spectral properties of two-particle interactions for particles feeling the same versus opposite magnetic-field directions. Thus any feasible route towards realizing the fractional QSH effect using a spin-dependent uniform magnetic field [29, 32] should strive to eliminate interactions between the opposite-spin components. If the opposite-spin interaction strength is weak, adiabatic passage between different correlated many-particle states is facilitated by adjusting the strength of a trapping potential. Our conclusions are supported by numerically obtained real-space-density profiles and angular-momentum-state occupation distributions for few-particle systems. The latter could also be utilized as blueprints for classifying images of correlated ultra-cold atom states.

Acknowledgments

Part of the motivation for this project came about from stimulating conversations that one of us (UZ) had with J. J. Heremans and R. Winkler at the 2011 Gordon Godfrey Workshop on Spins and Strong Correlations (Sydney, Australia, 24 – 28 October 2011). We would also like to thank M. Fleischhauer and A. H. MacDonald for useful discussions. OF was supported by the Marsden Fund Council from Government funding (contract No. MAU1205), administered by the Royal Society of New Zealand.

References

- [1] Bloch I, Dalibard J and Nascimbene S 2012 *Nat. Phys.* **8** 267–276
- [2] Hung C L, Gurarie V and Chin C 2013 *Science* **341** 1213–1215
- [3] Opanchuk B, Polkinghorne R, Fialko O, Brand J and Drummond P D 2013 *Ann. Phys. (Leipzig)* **525** 866–876
- [4] Dalibard J, Gerbier F, Juzeliūnas and Öhberg P 2011 *Rev. Mod. Phys.* **83** 1523
- [5] Lin Y J, Compton R L, Perry A R, Phillips W D, Porto J V and Spielman I B 2009 *Phys. Rev. Lett.* **102**(13) 130401
- [6] Lin Y J, Compton R L, Jiménez-García K, Porto J V and Spielman I B 2009 *Nature* **462** 628–632
- [7] Jimenez-Garcia K, LeBlanc L J, Williams R A, Beeler M C, Perry A R and Spielman I B 2012 *Phys. Rev. Lett.* **108**(22) 225303
- [8] Lin Y J, Jimenez-Garcia K and Spielman I B 2011 *Nature (London)* **471** 83–86
- [9] Galitski V and Spielman I B 2013 *Nature (London)* **494** 49–54
- [10] Goldman N, Kubasiak A, Gaspard P and Lewenstein M 2009 *Phys. Rev. A* **79**(2) 023624

- [11] Burrello M and Trombettoni A 2010 *Phys. Rev. Lett.* **105**(12) 125304
- [12] Estienne B, Haaker S M and Schoutens K 2011 *New J. Phys.* **13** 045012
- [13] Palmer R N and Pachos J K 2011 *New J. Phys.* **13** 065002
- [14] Goldman N, Satija I, Nikolic P, Bermudez A, Martin-Delgado M A, Lewenstein M and Spielman I B 2010 *Phys. Rev. Lett.* **105**(25) 255302
- [15] Béni B and Cooper N R 2011 *Phys. Rev. Lett.* **107**(14) 145301
- [16] Mei F, Zhu S L, Zhang Z M, Oh C H and Goldman N 2012 *Phys. Rev. A* **85**(1) 013638
- [17] Mazza L, Bermudez A, Goldman N, Rizzi M, Martin-Delgado M A and Lewenstein M 2012 *New J. Phys.* **14** 015007
- [18] Hasan M Z and Kane C L 2010 *Rev. Mod. Phys.* **82**(4) 3045–3067
- [19] Hasan M Z and Moore J E 2011 *Annu. Rev. Condens. Matter Phys.* **2** 55–78
- [20] Qi X L and Zhang S C 2011 *Rev. Mod. Phys.* **83**(4) 1057–1110
- [21] Kane C L and Mele E J 2005 *Phys. Rev. Lett.* **95**(22) 226801
- [22] Bernevig B A and Zhang S C 2006 *Phys. Rev. Lett.* **96**(10) 106802
- [23] Bernevig B A, Hughes T L and Zhang S C 2006 *Science* **314** 1757–1761
- [24] König M, Wiedmann S, Brüne C, Roth A, Buhmann H, Molenkamp L W, Qi X and Zhang S 2007 *Science* **318** 766–770
- [25] Murakami S, Nagaosa N and Zhang S C 2003 *Science* **301** 1348–1351
- [26] Sinova J, Culcer D, Niu Q, Sinitsyn N A, Jungwirth T and MacDonald A H 2004 *Phys. Rev. Lett.* **92**(12) 126603
- [27] Zhu S L, Fu H, Wu C J, Zhang S C and Duan L M 2006 *Phys. Rev. Lett.* **97**(24) 240401
- [28] Liu X J, Liu X, Kwek L C and Oh C H 2007 *Phys. Rev. Lett.* **98**(2) 026602
- [29] Beeler M C, Williams R A, Jiménez-García K, LeBlanc L J, Perry A R and Spielman I B 2013 *Nature* **498** 201–204
- [30] Aidelsburger M, Atala M, Lohse M, Barreiro J T, Paredes B and Bloch I 2013 *Phys. Rev. Lett.* **111**(18) 185301
- [31] Miyake H, Siviloglou G A, Kennedy C J, Burton W C and Ketterle W 2013 *Phys. Rev. Lett.* **111**(18) 185302
- [32] Kennedy C J, Siviloglou G A, Miyake H, Burton W C and Ketterle W 2013 *Phys. Rev. Lett.* **111**(22) 225301
- [33] Prange R E and Girvin S M (eds) 1990 *The Quantum Hall Effect* (New York: Springer)
- [34] MacDonald A H 1995 *Mesoscopic Quantum Physics* (Amsterdam: Elsevier Science) pp 659–720
Proceedings of the 1994 Les Houches Summer School, Session LXI
- [35] Haldane F D M 1990 *The Quantum Hall Effect* (New York: Springer) pp 303–352
- [36] Cooper N R 2008 *Adv. Phys.* **57** 539–616
- [37] Viefers S 2008 *J. Phys.: Condens. Matter* **20** 123202
- [38] Liu X J, Liu X, Kwek L C and Oh C H 2009 *Phys. Rev. B* **79**(16) 165301
- [39] Halperin B I 1983 *Helv. Phys. Acta* **56** 75–102
- [40] Reijnders J W, van Lankvelt F J M, Schoutens K and Read N 2002 *Phys. Rev. Lett.* **89**(12) 120401
- [41] Reijnders J W, van Lankvelt F J M, Schoutens K and Read N 2004 *Phys. Rev. A* **69**(2) 023612
- [42] Lan Y and Wan S 2012 *J. Phys: Condens. Matter* **24** 165503
- [43] Goerbig M 2012 *Eur. Phys. J. B* **85** 1–8
- [44] Levin M and Stern A 2009 *Phys. Rev. Lett.* **103**(19) 196803
- [45] Levin M, Burnell F J, Koch-Janusz M and Stern A 2011 *Phys. Rev. B* **84**(23) 235145
- [46] Qi X L 2011 *Phys. Rev. Lett.* **107**(12) 126803
- [47] Neupert T, Santos L, Ryu S, Chamon C and Mudry C 2011 *Phys. Rev. B* **84**(16) 165107
- [48] Haldane F D M 1988 *Phys. Rev. Lett.* **61**(18) 2015–2018
- [49] Tang E, Mei J W and Wen X G 2011 *Phys. Rev. Lett.* **106**(23) 236802
- [50] Sun K, Gu Z, Katsura H and Das Sarma S 2011 *Phys. Rev. Lett.* **106**(23) 236803
- [51] Neupert T, Santos L, Chamon C and Mudry C 2011 *Phys. Rev. Lett.* **106**(23) 236804
- [52] Ghaemi P, Cayssol J, Sheng D N and Vishwanath A 2012 *Phys. Rev. Lett.* **108**(26) 266801

- [53] Haldane F D M 1983 *Phys. Rev. Lett.* **51**(7) 605–608
- [54] Xu L L, Ren S and Heremans J J 2011 *Integr. Ferroelectr.* **131** 36–46
- [55] Juliá-Díaz B, Graß T, Barberán N and Lewenstein M 2012 *New J. Phys.* **14** 055003
- [56] Ho T L and Zhang S 2011 *Phys. Rev. Lett.* **107**(15) 150403
- [57] Ramachandhran B, Opanchuk B, Liu X J, Pu H, Drummond P D and Hu H 2012 *Phys. Rev. A* **85**(2) 023606
- [58] Ho T L 1998 *Phys. Rev. Lett.* **81**(4) 742–745
- [59] Wang C, Gao C, Jian C M and Zhai H 2010 *Phys. Rev. Lett.* **105**(16) 160403
- [60] Ohmi T and Machida K 1998 *J. Phys. Soc. Jpn.* **67** 1822–1825
- [61] Cooper N R and Wilkin N K 1999 *Phys. Rev. B* **60**(24) R16279–R16282
- [62] Wilkin N K and Gunn J M F 2000 *Phys. Rev. Lett.* **84**(1) 6–9
- [63] Viefers S, Hansson T H and Reimann S M 2000 *Phys. Rev. A* **62**(5) 053604
- [64] Popp M, Paredes B and Cirac J I 2004 *Phys. Rev. A* **70**(5) 053612
- [65] Cooper N R, van Lankvelt F J M, Reijnders J W and Schoutens K 2005 *Phys. Rev. A* **72**(6) 063622
- [66] Douglas J S and Burnett K 2011 *Phys. Rev. A* **84**(5) 053608